

Claire M. Cote · Keith L. Bristow
Philip B. Charlesworth · Freeman J. Cook
Peter J. Thorburn

Analysis of soil wetting and solute transport in subsurface trickle irrigation

Received: 18 June 2001 / Accepted: 30 September 2002 / Published online: 17 October 2003
© Springer-Verlag 2003

Abstract The increased use of trickle or drip irrigation is seen as one way of helping to improve the sustainability of irrigation systems around the world. However, soil water and solute transport properties and soil profile characteristics are often not adequately incorporated in the design and management of trickle systems. In this paper, we describe results of a simulation study designed to highlight the impacts of soil properties on water and solute transport from buried trickle emitters. The analysis addresses the influence of soil hydraulic properties, soil layering, trickle discharge rate, irrigation frequency, and timing of nutrient application on wetting patterns and solute distribution. We show that (1) trickle irrigation can improve plant water availability in medium and low permeability fine-textured soils, providing that design and management are adapted to account for their soil hydraulic properties, (2) in highly permeable coarse-textured soils, water and nutrients move quickly downwards from the emitter, making it difficult to wet the near surface zone if emitters are buried too deep, and (3) changing the fertigation strategy for highly permeable coarse-textured soils to apply nutrients at the beginning

of an irrigation cycle can maintain larger amounts of nutrient near to and above the emitter, thereby making them less susceptible to leaching losses. The results demonstrate the need to account for differences in soil hydraulic properties and solute transport when designing irrigation and fertigation management strategies. Failure to do this will result in inefficient systems and lost opportunities for reducing the negative environmental impacts of irrigation.

Introduction

The irrigation industry is facing increasing pressure to improve the efficiency of irrigation water use and to reduce environmental impacts such as rising groundwater tables, salinisation and groundwater pollution. The use of trickle or drip irrigation on field-grown crops has become quite a common practice in agricultural production in various parts of the world, as they are seen as a means to achieve sustainable irrigation management practices.

Trickle irrigation systems consist of small emitters, either buried or placed on the soil surface, which discharge water at a controlled rate. Water infiltration takes place in the region directly around the emitter, which is small compared with the total soil volume of the irrigated field. As a result, three-dimensional transient infiltration occurs. This differs from more traditional techniques of flood or sprinkler irrigation, where water infiltrates through most or all of the soil surface area, and water infiltration can usually be adequately simulated by one-dimensional vertical movement (Brandt et al. 1971; Bresler 1977). Moreover, trickle irrigation systems are capable of delivering water and nutrients to the soil in small quantities at any time with no great additional economic cost. This allows maintenance of a partially wetted soil volume with conditions near optimal for crop growth. As the frequency of irrigation increases, the infiltration period becomes a more important part of the irrigation cycle. Detailed knowledge of the water-holding

Communicated by J. Annandale

C. M. Cote
CSIRO Land and Water, PMB Aitkenvale,
Townsville, Qld 4814, Australia

K. L. Bristow (✉) · P. B. Charlesworth
CSIRO Land and Water and CRC for Sustainable
Sugar Production, PMB Aitkenvale, Townsville,
Qld 4814, Australia
E-mail: Keith.Bristow@csiro.au
Tel.: +61-7-47538596
Fax: +61-7-47538650

F. J. Cook
CSIRO Land and Water and CRC for Sustainable
Sugar Production, 12 Meiers Rd, Indooroopilly,
Qld 4068, Australia

P. J. Thorburn
CSIRO Sustainable Ecosystems and CRC for Sustainable
Sugar Production, 306 Carmody Rd,
St Lucia, Qld 4067, Australia

capacity of the soil is less important for the design of trickle-irrigated systems than for other systems. The hydraulic properties, however, are critical because they control the infiltration phase (Rawlins 1973; Bresler 1978). Irrigation management under high-frequency water applications involves controlling the quantity of water passing through the root zone by regulating the trickle discharge rate according to the soil hydraulic properties, and minimising deep percolation and leaching of nutrients and other chemicals from the root zone.

While some guidelines have been published to help growers install, maintain and operate trickle irrigation systems (see, for instance, Hanson et al. 1996), there are at present few, if any, clear guidelines for designing and managing trickle irrigation systems that account for differences in soil hydraulic properties. Hence, systems are often designed to an economic optimum in terms of the engineering, which may not deliver the best environmental outcomes. In addition to experiments, theoretical analysis and simulations of trickle irrigation are needed to help develop more robust installation and management guidelines.

The design and management of trickle irrigation requires an understanding of water and solute distribution patterns, which may be described and predicted by solutions of the governing flow equations (Thorburn et al. 2000; Bristow et al. 2000). Analytical solutions of the three-dimensional Richards' equation have been derived for steady infiltration from buried point sources and cavities (Philip 1968, 1984), from point sources placed at the soil surface (Raats 1971), and from shallow circular ponds placed at the soil surface (Wooding 1968). These analytical solutions deal with axially symmetric steady state flow. They describe well the early stages of infiltration and provide an estimate of the water content behind the wetting front (Clothier and Scotter 1982). Although easy to implement, they deal mainly with design considerations of the trickle source.

To improve irrigation management practices, more dynamic approaches are needed. Analytical solutions of transient axi-symmetrical infiltration have been developed for point sources placed at the soil surface (Warrick 1974), which were later tested against experimental data (Revol et al. 1997), and for strip and disc sources (Warrick and Lomen 1976). These solutions more accurately captured the highly dynamic conditions associated with the "pulsed" water input often used in trickle irrigation (Coelho and Or 1997). However, these solutions are based on limiting assumptions pertaining to the source configuration, the linearisation of the flow equation, homogeneous soil hydraulic properties, and they deal with water flow only. Hence, their application in trickle management is limited. Numerical solutions of the flow equations have been developed for surface point sources, thereby widening the range of application (Bresler et al. 1971; Brandt et al. 1971), and including solute transport (Bresler 1975). Limitations of these solutions are an inaccurate treatment of the surface boundary condition (Lafolie et al. 1989a, 1989b).

Theoretical analyses can only yield design and management guidelines if they can closely match the system and the processes taking place. Considerable progress has been made in the conceptual understanding and mathematical description of water flow, solute transport, and root water uptake in trickle systems. This knowledge has now been integrated in various software packages, including HYDRUS2D, which simulates three-dimensional axially symmetric water flow, solute transport, and root water and nutrient uptake based on finite-element numerical solutions of the flow equations (Simunek et al. 1999). HYDRUS2D enables implementation of a wide range of boundary conditions, irregular boundaries, and soil heterogeneities. The package is supported by an interactive graphics-based user interface for data pre-processing, generation of the calculation mesh, and graphics presentation of the results, and is therefore reasonably easy to use. With these attributes, HYDRUS2D is a good tool for analysing design features and management of trickle irrigation systems.

In this paper, we show how HYDRUS2D simulations can be used to analyse water flow and solute transport in trickle irrigation systems consisting of buried spherical sources. We pay particular attention to

- the influence of soil hydraulic properties on wetting patterns,
- the influence of trickle discharge rate on wetting patterns,
- the influence of pulsed input on wetting patterns,
- the timing of solute application on the resultant distribution of solutes within the root zone.

Our results challenge the common perceptions that (1) high-frequency irrigation or "pulsing" increases the lateral extent of the wetting patterns, and (2) that fertigation should be applied at the end of an irrigation cycle to minimise nutrient leaching.

Theory

Consider a field that is irrigated by a set of emitters spaced at regular intervals $2R$ at depth Z_e as shown in Fig. 1. Due to the symmetry of the emitter layout, and assuming that each emitter discharges water at the same flow rate, a 1-ha field can be subdivided into identical volume elements of length and width $2R$ and depth Z , with a trickle emitter placed at depth Z_e on the plane of symmetry. It is assumed that the trickle emitter can be represented as a small sphere of radius ρ [L]. In order to describe water patterns in an entire field, it is sufficient to analyse the flow in this single volume element. Because of the axial symmetry around the vertical axis, the infiltration process can be viewed as an axi-symmetrical flow, with the radius r [L] and the depth z [L] as key variables. Three-dimensional axi-symmetrical flow in variably saturated, rigid, isotropic porous media can be

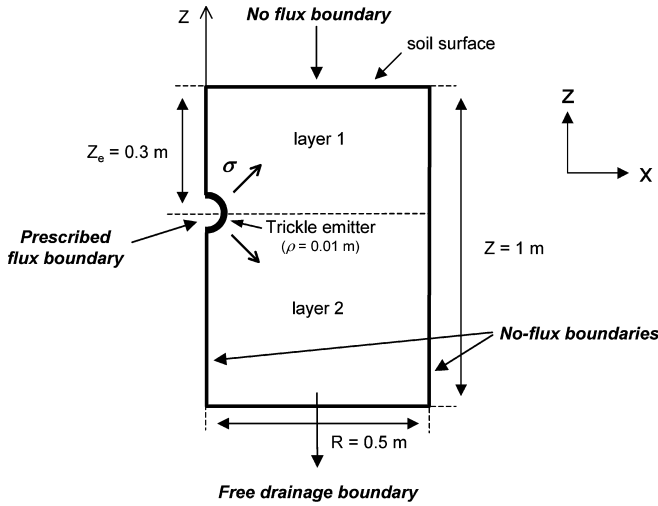


Fig. 1 Schematic showing the physical layout of the trickle irrigation system implemented in HYDRUS2D, including the boundary conditions. The emitter is represented by *half a sphere* and the complete irrigation system is obtained by rotation around the z -axis (note that the schematic is not to scale)

described by the following modified form of Richards' equation

$$\frac{\partial \theta}{\partial t} = \frac{\partial}{\partial r} \left(K(h) \frac{\partial h}{\partial r} \right) + \frac{K(h)}{r} \frac{\partial h}{\partial r} + \frac{\partial}{\partial z} \left(K(h) \left(\frac{\partial h}{\partial z} + 1 \right) \right) \quad (1)$$

where θ [L^3L^{-3}] is the volumetric water content, h [L] is the pressure head, t [T] is time, r [L] is the radial coordinate, z [L] is the vertical coordinate taken positive upwards, and K [LT^{-1}] is the unsaturated hydraulic conductivity.

Fluxes of solute in soil are controlled by physical transport, chemical interactions and biological processes. In this paper, we are primarily concerned with the influence of soil properties and trickle discharge on the physical transport of solute, and we ignore chemical interactions and biological processes. In a homogeneous porous medium, three-dimensional axi-symmetrical transport of a single non-reactive ion can be described with the polar coordinates form of the widely used advection–dispersion equation (Bear 1972)

$$\begin{aligned} \frac{\partial(\theta C)}{\partial t} = & \frac{\partial}{\partial r} \left(\theta D_{rr} \frac{\partial C}{\partial r} + \theta D_{rz} \frac{\partial C}{\partial z} \right) + \frac{1}{r} \left(\theta D_{rr} \frac{\partial C}{\partial r} + \theta D_{rz} \frac{\partial C}{\partial z} \right) \\ & + \frac{\partial}{\partial z} \left(\theta D_{zz} \frac{\partial C}{\partial z} + \theta D_{rz} \frac{\partial C}{\partial r} \right) - \left(\frac{\partial q_r C}{\partial r} + \frac{q_r C}{r} + \frac{\partial q_z C}{\partial z} \right) \end{aligned} \quad (2)$$

Here C [ML^{-3}] is solute concentration in the soil water, q_r and q_z [LT^{-1}] are the components of the volumetric flux density, D_{rr} , D_{zz} and D_{rz} [L^2T^{-1}] are the components of the dispersion tensor. These components are given by (Bear 1972)

$$\begin{aligned} \theta D_{rr} &= \varepsilon_L \frac{q_r^2}{|q|} + \varepsilon_T \frac{q_z^2}{|q|} + \theta \tau D_o \\ \theta D_{zz} &= \varepsilon_L \frac{q_z^2}{|q|} + \varepsilon_T \frac{q_r^2}{|q|} + \theta \tau D_o \\ \theta D_{rz} &= (\varepsilon_L - \varepsilon_T) \frac{q_r q_z}{|q|} \end{aligned} \quad (3)$$

where $|q|$ [LT^{-1}] is the absolute value of the volumetric flux density, ε_L and ε_T [L] are the longitudinal and transversal dispersivities, D_o [L^2T^{-1}] is the molecular diffusion coefficient of the solute in free water, and τ is the tortuosity factor. In this study, Eqs. 1, 2 and 3 are solved numerically using HYDRUS2D (Simunek et al. 1999) with initial and boundary conditions that closely reproduce trickle irrigation systems (see Materials and methods section).

There are also analytical solutions of Eq. 1 that can be used to estimate the dimensions of the wetted soil volume under a trickle system for steady-state flow. For instance, based on the quasi-linear analysis of steady three-dimensional unsaturated flow, Philip (1984) calculated the dimensionless travel time T of the wetting front away from a buried point source as a function of the dimensionless vertical distance Z_+ (downwards from the source) and Z_- (upwards from the source) and the dimensionless radial distance R as

$$T = \frac{(Z_+^2 - Z_-^2)}{2} + \frac{\ln(1 + 2Z_+)}{4} \quad (4a)$$

$$T = \frac{1}{2} [e^{2Z_-} (1 - 2Z_- + 2Z_-^2) - 1] \quad (4b)$$

$$\begin{aligned} T(0, R) = e^R \left[R^2 - R + \frac{1}{2} (1 - R - \ln(2)) \cdot \ln(2e^R - 1) \right. \\ \left. - \frac{1}{2} L(2e^R) - \frac{\pi^2}{24} \right] \end{aligned} \quad (5)$$

$$Z_+ = z_+ / 2\lambda_c \text{ and } Z_- = z_- / 2\lambda_c \quad (6)$$

$$R = r / 2\lambda_c \quad (7)$$

$$T = \frac{Qt}{16\pi(\langle \theta \rangle - \theta_{in})\lambda_c^3} \quad (8)$$

L is the dilogarithm defined as

$$L(x) = - \int_1^x \frac{\ln x}{x-1} dx \quad (9)$$

In the above, Q [L^3T^{-1}] is the volumetric trickle discharge rate, $\langle \theta \rangle$ is the average volumetric water content in the soil behind the wetting front, θ_{in} is the initial volumetric water content, $E_i(x)$ is the exponential integral, and λ_c is the macroscopic capillary length scale defined as (Philip 1968, 1984; White and Sully 1987)

$$\lambda_c = \frac{\int_{h_{in}}^{h_o} K(h) dh}{K(h_o) - K(h_{in})} \quad (10)$$

where h_o is the pressure head at the supply surface and h_{in} is the initial pressure head. Philip's (1984) work has been used to provide predictions of the radius and depth of the wetting patterns in previous studies (Revol et al. 1997; Thorburn et al. 2000). While they only yield a simplified solution of Eq. 1 compared with the numerical solutions used in this study, they do provide a good theoretical framework with which we compared our results.

Materials and methods

We used the HYDRUS2D software package (Simunek et al. 1999) to simulate three-dimensional axi-symmetric water flow and solute transport in variably saturated soils. We present here the information on which our simulations are based.

Processes

The processes included in the simulations were water flow and solute transport. The objectives of the simulations were to analyse various scenarios to assist with development of guidelines for minimising the environmental impact of trickle irrigation through better prediction and management of deep drainage and solute leaching. Because of this focus on minimising environmental risk, we are most interested in the "worst" case scenario in which there is no root uptake of water or solute, and the risk of solute leaching is increased.

System geometry

The simulations were for a soil profile of depth $Z=1$ m, width $2R=1$ m, with a trickle emitter of radius $\rho=0.01$ m placed at depth $Z_e=0.3$ m on the plane of symmetry. This choice of emitter spacing yields 10,000 emitters per hectare, which is representative of many trickle systems. Figure 1 shows the dimensions we used in our simulations as well as the imposed boundary conditions. No flux was allowed through the surface and lateral boundaries, and a deep drainage boundary condition was used for the bottom boundary. The system was conceptually divided into two layers, corresponding to the soil volume located above and below the emitter, so that water and solute mass balance could be determined for each layer. This also allowed us to illustrate the position of solute plumes within the soil profile.

The finite element dimensions were adjusted to meet our needs, with smaller elements ($\cong 1.5$ mm²) around the emitter where fast change in fluxes and variables occur, and larger elements ($\cong 3$ cm²) away from the emitter. The sizes of the elements are governed by the number of nodes on the system boundary (the more nodes, the finer the elements). We chose a total of 120 nodes on the outer boundary, with a much higher density of nodes around the emitter (12 nodes on the emitter, 12 nodes along the plane 10 cm above and below the emitter).

Initial and boundary conditions

Initial condition

We set the initial distribution of the pressure head h within the flow domain to be uniform throughout the soil profile

$$h(x, z) = h_{in} = -30 \text{ m}, \quad t = 0 \quad (11)$$

Boundary conditions

For the purpose of investigating the influence of trickle discharge, soil hydraulic properties, and frequency of water input on wetting patterns, a constant flux boundary condition at the surface of the spherical emitter was used. This took the form

$$\left(K(h) \frac{\partial h}{\partial r} \right) u_r + \left(K(h) \left(\frac{\partial h}{\partial z} + 1 \right) \right) u_z = \sigma(t) \quad r = \rho; \quad 0 < t \quad (12)$$

where σ [LT⁻¹] is a prescribed function of time, giving the value of the flux at the surface of the spherical emitter, and u_r , u_z are the components of the outward unit vector normal to this boundary. The value of σ was assigned one of four different values. These values were chosen to demonstrate the impact of both the soil hydraulic properties and flow rate on soil wetting patterns:

Flux 1 $\sigma = 1.31$ m/h. The total volumetric flux Q is

$$Q = 4\pi\rho^2 \sigma = 1.26 \times 10^{-3} \times 1.31 = 1.65 \times 10^{-3} \text{ m}^3/\text{h} = 1.65 \text{ l/h} \quad (13)$$

This value of 1.65 l/h is typical of that used in the Australian sugar industry.

Flux 2 $\sigma = K_s$ m/h, so that Q depends on soil type; we had $\sigma = 0.297$ m/h for the sand ($\cong 0.38$ l/h), and $\sigma = 0.0025$ m/h for the silt ($\cong 0.003$ l/h).

Flux 3 $\sigma = K_s/2$ m/h.

Flux 4 $\sigma = K_s/5$ m/h.

In this study, we assume that the water table is situated far below the domain of interest and therefore have a free drainage boundary condition at the base of the soil profile ($z=0$). This is treated as a unit vertical hydraulic gradient in HYDRUS2D. At the surface and on the sides of the soil profile ($z=Z$, $r=0$ and $r=R$), we assumed that no flux of water took place and chose a no-flux boundary condition, which in HYDRUS2D is specified for impermeable boundaries where the flux is zero perpendicular to the boundary. More information concerning implementation of these boundary conditions can be found in the HYDRUS2D user manual (Simunek et al. 1999).

Boundary conditions for solute transport

We chose the initial solute concentration within the flow domain to be uniform and equal to zero throughout the soil profile

$$c(r, z) = c_{in} = 0 \quad t = 0 \quad (14)$$

Solute is applied with irrigation water and a third-type boundary condition is used to prescribe the concentration flux along the boundary of the emitter, of the form

$$-(\theta D_{rr} \frac{\partial C}{\partial r} + \theta D_{rz} \frac{\partial C}{\partial z}) + q_r C = q_r C_o \quad (15)$$

$$-(\theta D_{zz} \frac{\partial C}{\partial z} + \theta D_{rz} \frac{\partial C}{\partial r}) + q_z C = q_z C_o$$

where C_o [ML⁻³] is the concentration of the incoming fluid, set to 2.3 g/l.

Soil hydraulic properties

The soil properties needed are the highly non-linear water retention $\theta(h)$ and hydraulic conductivity $K(h)$ functions. In this study we used the van Genuchten (1980) analytical model for the soil hydraulic properties

$$\theta(h) = \begin{cases} \theta_r + \frac{\theta_s - \theta_r}{(1 + |\alpha h|)^m} & h < 0 \\ \theta_s & h \geq 0 \end{cases} \quad (16)$$

$$K(h) = K_s S_e^l \left(1 - \left(1 - S_e^{1/m} \right)^m \right)^2 \quad (17)$$

$$S_e = \frac{\theta - \theta_r}{\theta_s - \theta_r} \quad (18)$$

$$m = 1 - \frac{1}{n} \quad n > 1 \quad (19)$$

where l is the pore connectivity parameter (equal to 0.5 for most soils), θ_s [$L^3 L^{-3}$] is saturated water content, θ_r [$L^3 L^{-3}$] is residual water content, α [L^{-1}] and n are empirical factors, and K_s [LT^{-1}] is saturated hydraulic conductivity. Simulations of water and solute movement were carried out for three soils with contrasting physical properties: a highly permeable coarse-textured sand, a medium permeability fine-textured silt, and a duplex soil. The duplex soil consisted of an upper 30 cm layer of the medium permeability silt and a lower 70 cm layer of a low permeability fine-textured silty clay loam. The parameters θ_s , θ_r , α , n and K_s for these soils were taken from the HYDRUS2D soil catalogue. Their values are listed in Table 1. Figure 2 shows the water retention and hydraulic conductivity functions for the three soils. These hydraulic properties illustrate the effect different soil properties can have on water infiltration and solute movement in trickle irrigation systems.

Solute transport properties

Determination of the components of the dispersion tensor D_{rr} , D_{zz} and D_{rz} requires knowledge of the molecular diffusion coefficient of the solute in free water D_o and the longitudinal and transversal dispersivities ε_L and ε_T (Eq. 3). We used $D_o = 0.068 \text{ cm}^2/\text{h}$ [which is the value of the diffusion coefficient of NO_3^- in solution at 25°C (Weast 1978)] to mimic nitrate diffusion. As an approximation, we took the longitudinal dispersivity equal to one-tenth of the profile depth Z , as this is supported by previous studies that addressed characterisation of solute transport in soils (e.g. Beven et al. 1993; Cote et al. 2001). This gives $\varepsilon_L = 0.1 \text{ m}$. We also set $\varepsilon_T = \varepsilon_L/10 = 0.01 \text{ m}$ (Bear 1972).

Irrigation and fertigation strategies

Irrigation simulations were selected to represent typical systems encountered in the Australian sugarcane industry, and these were then compared with alternative methods to demonstrate what can be achieved by using different management strategies. In our simulations, all irrigation cycles consisted of 5 h of water application. During this 5 h period, the emitter discharged water at a total volumetric rate Q (Eq. 13) and the total volume of applied water V_w was

$$V_w = 4\pi\rho^2 \times \sigma \times 5 \quad (20)$$

Two irrigation scenarios were simulated. The first involved “continuous” irrigation, with water applied continuously for 5 h. The second involved “pulsed” irrigation, with water applied intermittently in 30 min periods (i.e. 0.5 h irrigation, followed by 0.5 h of no irrigation) for a total duration of 10 h. The total volume of applied water was the same in both cases.

Table 1 Parameters describing the soil hydraulic properties for the three soils used in this study (θ_s is saturated water content, θ_r is residual water content, α and n are empirical factors and K_s is the saturated hydraulic conductivity)

	θ_r	θ_s	$\alpha \text{ (cm}^{-1}\text{)}$	n	$K_s \text{ (cm/h)}$
Sand	0.045	0.43	0.145	2.68	29.7
Silt	0.034	0.46	0.016	1.37	0.25
Silty clay loam	0.089	0.43	0.010	1.23	0.07

For the continuous irrigation scenario, solute was applied as a solution of concentration C_o during a 1 h-long solute pulse within the irrigation event. The timing of the solute application depended on the fertigation strategy. Two fertigation strategies were addressed. In fertigation strategy E (Fig. 3), the solute is applied at the End of the irrigation cycle, i.e. at $t = 4 \text{ h}$. In fertigation strategy B (Fig. 3), the solute pulse is applied at the Beginning of the irrigation cycle, i.e. at $t = 0 \text{ h}$, so that the solute is applied to a much drier soil than with fertigation strategy E.

In the case of pulsed irrigation, solute is applied as a solution of concentration C_o during two half-hour-long solute pulses. In fertigation strategy E_p, solute is applied during the last two half-hours of the irrigation cycle and in fertigation strategy B_p, it is applied during the first two half-hours of the irrigation cycle (Fig. 4). The total amount of solute applied per irrigation event was equivalent to 40 kg N/ha, which is typical of what is used in many trickle systems within the Australian sugarcane industry.

Results

Influence of soil hydraulic properties on wetting patterns

Numerical simulations of water flow in the sand, silt and duplex soils are given in Fig. 5. This figure shows simulated water content patterns in the three soils where water was applied continuously with Flux 2 ($\sigma = K_s$). For the duplex soil, the flux density σ was

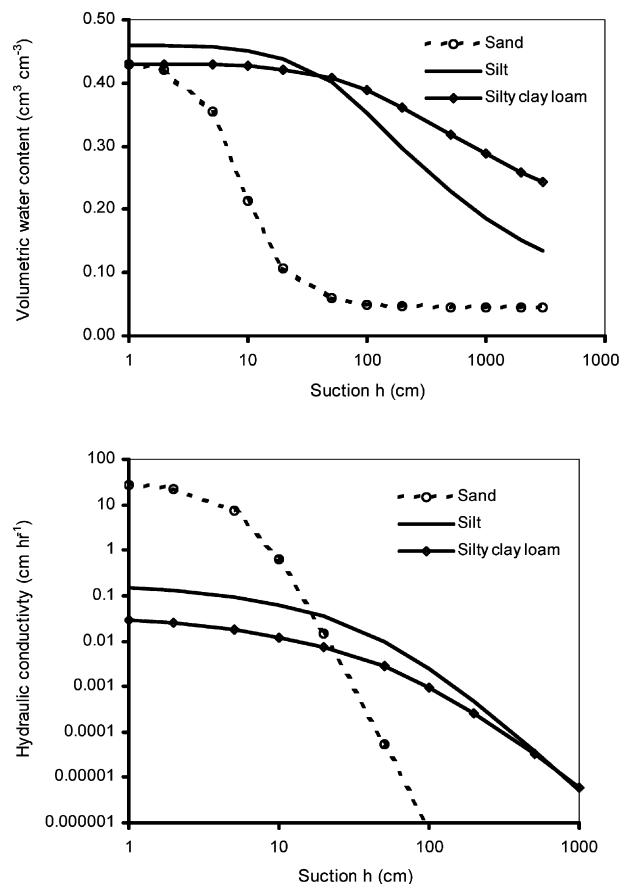


Fig. 2 Soil hydraulic properties for the three soils used in this study

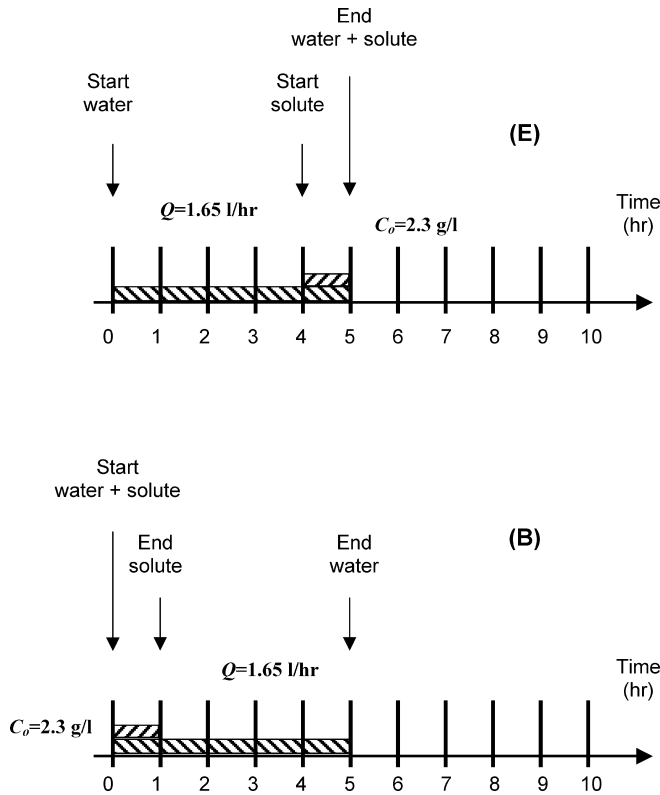


Fig. 3 Schematic showing fertigation strategy (E) in which solute is applied at the End of the irrigation cycle, and (B) in which solute is applied at the Beginning of the irrigation cycle

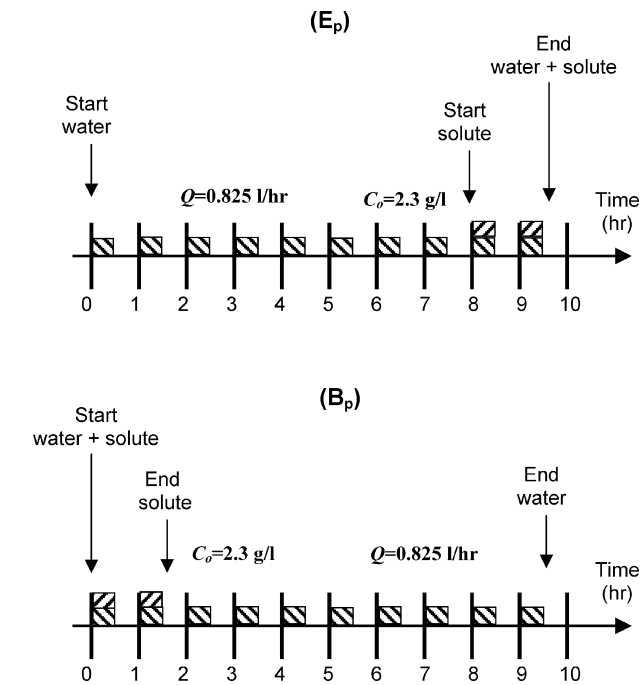


Fig. 4 Fertigation strategies (E_p) and (B_p) for pulsed irrigation, with water being applied during the first half-hour of every hour

taken equal to the saturated conductivity of the silt. Since the flux value was adjusted to the soil hydraulic properties, we show the patterns for the same total

amount of infiltrated water (=6.3 l). The figure displays the spatial distribution of the water content by means of a colour spectrum. Note that limitation in the software means that the colour spectrum scale can be different for each soil. Note that the initial condition was set with a uniform pressure head distribution $h_{in} = -30 \text{ m}$. The water content at this pressure head is θ_{in_2} which equals $0.045 \text{ cm}^3/\text{cm}^3$ in the sand, $0.135 \text{ cm}^3/\text{cm}^3$ in the silt, and $0.244 \text{ cm}^3/\text{cm}^3$ in the silty clay loam (Fig. 2). The water content distribution in the wetted zone therefore contrasts with the background, which remained at θ_{in} .

In the highly permeable sand, the wetting pattern is elliptical, with the wetted depth larger than the wetted radius resulting in more water below the emitter plane than above (94% of the applied water is below the emitter). There is little movement of water up into the zone above the emitter with water contents in the top 15 cm of the soil profile remaining equal to θ_{in} . In the low permeability silt, the wetting pattern is roughly spherical. After 6.3 l of cumulative infiltration, the wetting front has reached the soil surface. A similar amount of water is stored above and below the emitter.

In the duplex soil, water does not easily penetrate into the slowly permeable silty clay loam layer below the emitter, so most of the water moves up into the silt layer, above the emitter. The initial water content of the silty clay loam was much higher than that of the silt, so the silty clay loam layer remains wetter than most of the silt layer. However, the water in this layer is held at a higher suction (Fig. 2) and is not as readily available for plant uptake.

Figure 6 compares the wetted radius and the wetted depth in the sand and silt at 6.3 l of cumulative infiltration, as calculated using the numerical simulations. Figure 6 shows plots of the water content as a function of the radial distance r along the line $z=30 \text{ cm}$ (i.e. at the emitter depth), and as a function of the vertical distance z along the line $r=0$ (i.e. right under the emitter). The location of the wetting front can be defined as a line of maximum gradient in water content (Bresler et al. 1971). In Fig. 6, the maximum gradient in water content can be observed at $r=0.25 \text{ m}$ and $z=0.50 \text{ m}$ for the sand, and at $r=0.35 \text{ m}$ and $z=0.35 \text{ m}$ for the silt, which yields the wetted radius and wetted depth for these two soils. This confirms that the wetting pattern in the slowly permeable silt is circular, with the wetted radius equal to the wetted depth, the wetted depth in the sand is much greater than in the silt, and the wetted radius in the silt is greater than that in the sand. In the finer-textured soil, at the initial water suction of -30 m , there is less available air-filled pore space than in the coarse-textured soil (Fig. 2), and this forces the water to move further from the emitter. Also, the wetting front is less sharp in the silt than in the sand, with Fig. 6 showing much smoother curves for the silt than the sand.

To quantify the influence of soil hydraulic properties on wetting patterns, previous analytical studies have

Fig. 5 Simulated water content distribution around the emitter for 6.3 l of cumulative infiltration with $\sigma = K_s$ for A sand, B silt and C duplex soil

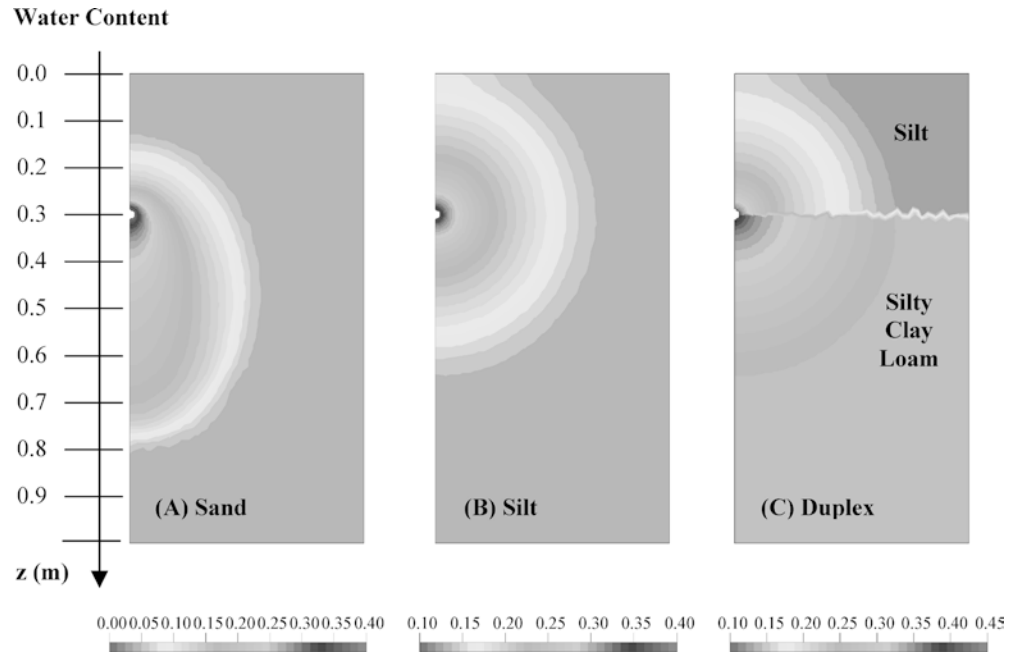
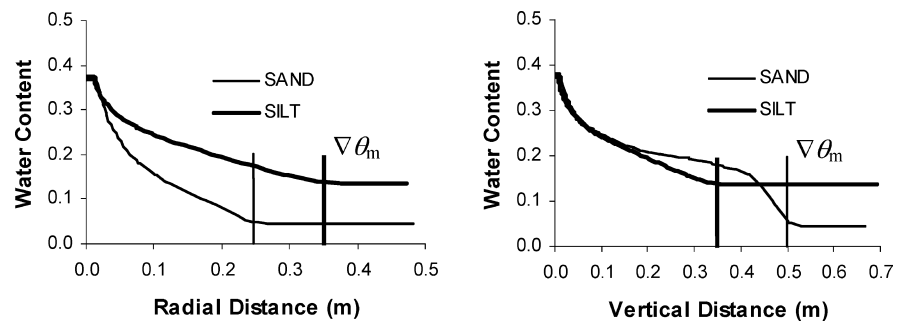


Fig. 6 Wetted radius and wetted depth in the sand and silt for 6.3 l of applied water with $\sigma = K_s$



used the macroscopic capillary length scale λ_c as defined in Eq. 10. The associated sorptive time scale is

$$t_c = \frac{(\theta_o - \theta_{in}) \times \lambda_c}{K(h_o) - K(h_{in})} \quad (21)$$

with $\theta_o = \theta(h_o) = \theta_s$ in our simulations. The macroscopic capillary length scale λ_c is a measure of the relative importance of gravity and capillarity for water movement in soil. Slowly permeable fine-textured materials, where capillarity tends to dominate, have large λ_c values, while highly permeable coarse-textured soils, where gravity effects manifest themselves more readily, have small λ_c values (Philip 1968). In the sand, $\lambda_c = 3.6$ cm and in the silt $\lambda_c = 8.3$ cm, with $t_c = 0.05$ h in the sand and $t_c = 14$ h in the silt. Hence in the highly permeable sand, gravity dominates and the wetted depth is much larger than the wetted radius whereas in the slowly permeable silt, capillarity dominates and the wetted pattern is more circular. It is also important to emphasise the effect of soil hydraulic properties on the time-scale involved with the infiltration process. The sorptive time scale in the silt is

280 times greater than that in the sand. Indeed, 6.3 l of water had infiltrated after 17 h in the sand, but only after 2,000 h in the silt. The infiltration process is several orders of magnitude slower in low permeability fine-textured materials than in high permeability coarse-textured ones.

Both the analytical and numerical analyses show that in highly permeable coarse-textured soils such as the sand used in this study, water drains easily and quickly from the root zone because gravity dominates. This can exacerbate off-site impacts, such as increased recharge and/or pollution of groundwater systems. In slowly permeable fine-textured materials such as the silt, water is held within typical root zones and as such would normally be readily available for plant uptake. However, water infiltrates in these soils slowly, and irrigation would have to be adapted to match the infiltration time scale. The results also show that trickle irrigation in a duplex soil could be ideal if appropriate management is used so that water will be readily available within the root zone with limited drainage losses.

Influence of trickle discharge rate on wetting patterns

Examples of water content distribution for three cases of trickle discharge rates (Flux 2, 3, 4) are given in Fig. 7 for the highly permeable sand and in Fig. 8 for the slowly permeable silt. In the sand, the water content distribution is shown at two values of cumulative infiltration, 10 l and 40 l. In the silt, it is shown at 1.6 l and 6.3 l of cumulative infiltration. To help quantify the influence of trickle discharge rate on wetting patterns, Fig. 9 gives plots of the water content as a function of the radial distance r along the line $z=30$ cm and as a function of the vertical distance z along the line $r=0$ for 1.6 l of cumulative infiltration. Note that the plots in Fig. 9 are deduced from the two-dimensional patterns given in Figs. 7 and 8. It is worth noting that in the medium and low permeability fine-textured soils, the silt and the silty clay loam, we could not run simulations with Flux 1 ($\sigma = 1.65$ l/h, a commonly used rate) as this

discharge rate was too high relative to the intake rate of these soils, resulting in failure of the numerical model. This highlights further the influence of soil hydraulic properties on trickle irrigation, and the need to accommodate these differences when designing and managing trickle irrigation systems.

As the trickle discharge rate decreases, the wetted radius increases (Fig. 7). This is highlighted by the plots in Fig. 9 where the wetted radius at 10 l of cumulative infiltration is 28 cm for $\sigma = K_s$, 30 cm for $\sigma = K_s/2$, and 35 cm for $\sigma = K_s/5$. The same result is found for the silt, with the wetted radius at 1.6 l of cumulative infiltration equal to 20 cm for $\sigma = K_s$, 25 cm for $\sigma = K_s/2$, and 29 cm for $\sigma = K_s/5$. These data concur with results of previous studies (Bresler 1978). The wetted depth increases with decreasing discharge rate as well. In the sand, at 10 l of cumulative infiltration, the wetted depth is 50 cm for $\sigma = K_s$, 60 cm for $\sigma = K_s/2$, and 65 cm for $\sigma = K_s/5$. In the silt, at 1.6 l of cumulative infiltration, the wetted depth is

Fig. 7 Simulated water content distribution in the sand with $\sigma = K_s$, $\sigma = K_s/2$, $\sigma = K_s/5$ for
A 10 l of applied water and
B 40 l of applied water

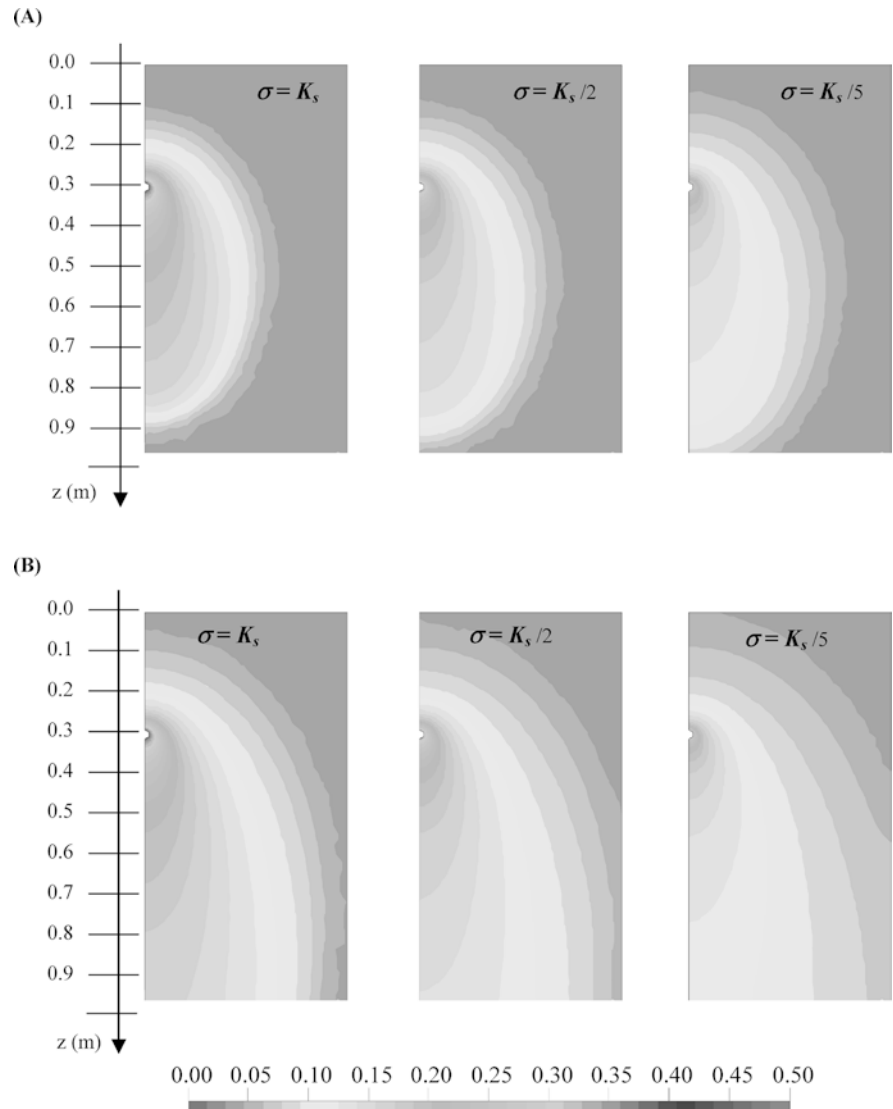
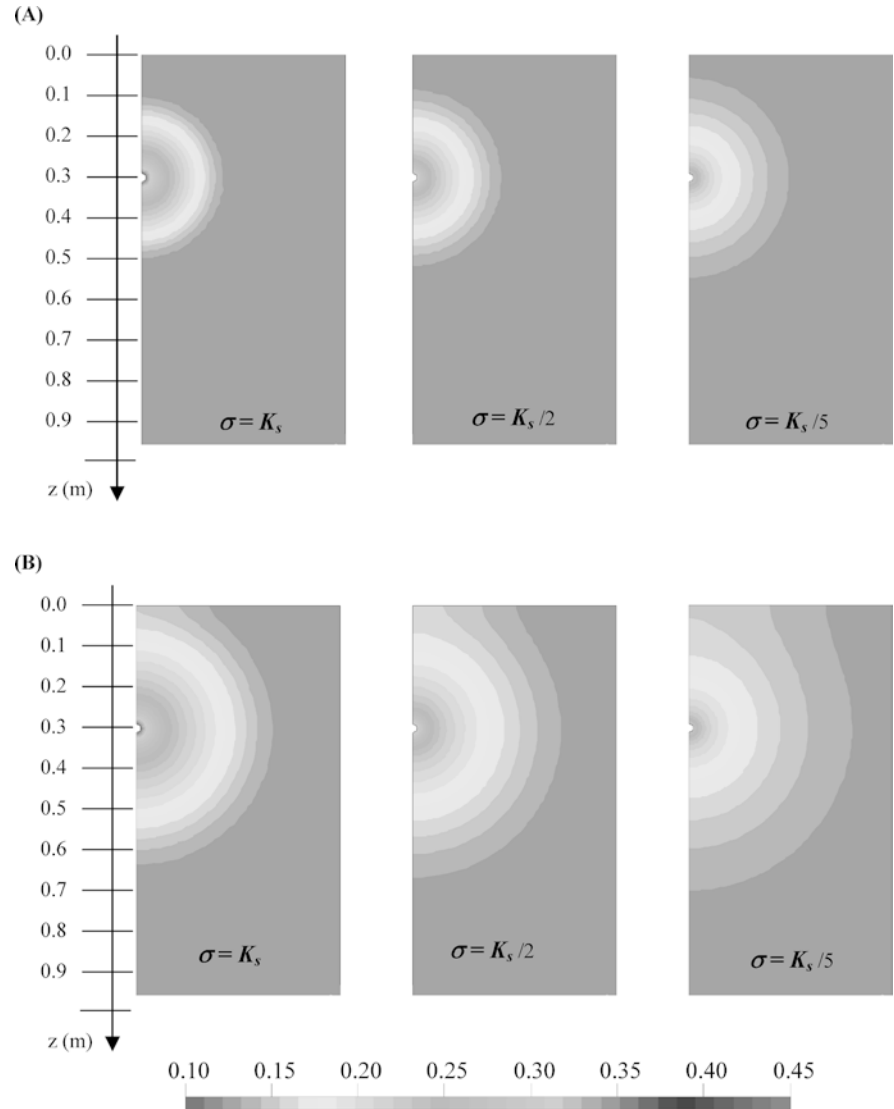


Fig. 8 Simulated water content distribution in the silt with $\sigma = K_s$, $\sigma = K_s/2$, $\sigma = K_s/5$ for **A** 1.6 l of applied water, and **B** 6.3 l of applied water



20 cm for $\sigma = K_s$, 22 cm for $\sigma = K_s/2$, and 25 cm for $\sigma = K_s/5$. This contradicts the findings of Bresler (1978), who found that an increase in the rate of discharge resulted in a decrease in the vertical component of the wetted soil depth. However, the rates of discharge they used were several orders of magnitude greater than ours (4 l/h and 20 l/h) and their soil was much more permeable, which could explain the discrepancies. Figure 9 also shows that the gradients of water content increase as the rate of discharge increases, with much sharper gradients at higher flow rates.

These counterintuitive results can be better understood by examining analytical studies of trickle irrigation, where the wetting patterns from a buried source can be described by Eqs. 4a, 4b, 5, 6, 7 and 8. Water content distributions in Figs. 7 and 8 are plotted at constant cumulative infiltration, i.e. at constant Qt . From Fig. 9, it is clear that the average water content $\langle \theta \rangle$ decreases as the flow rate decreases, so that T increases when the flow rate decreases.

Wetting fronts reach the same distance when dimensionless times are the same. Greater T values mean greater distances. Hence, when the flow rate decreases, the dimensionless time increases and so do the wetted radius and the wetted depth. From a more physically intuitive point of view, the time t needed to reach the amount of cumulative infiltration Qt is greater when Q is smaller. Hence, a decrease in discharge rate leads to a greater time needed to reach a given amount of infiltrated water and thus to a greater spread of water and greater wetted radius.

At the high value of cumulative infiltration (40 l) in the highly permeable sand, Fig. 10 shows that drainage increases as the rate of discharge decreases. At 40 l of cumulative infiltration, drainage is 15.3 l for Flux 4, 13.2 l for Flux 3 and 11.5 l for Flux 2. There is a 28% increase in drainage at this particular value of cumulative infiltration when the lowest rate of trickle discharge is used. In the slowly permeable silt, as the rate of discharge increases, the spread of water

Fig. 9 Water content at $z = -30$ cm as a function of radial distance r , and water content at $r = 0$ as a function of vertical distance z . Data are for three different flow rates (Flux 2, 3, 4) involving 10 l of applied water in the sand and 1.6 l of applied water in the silt

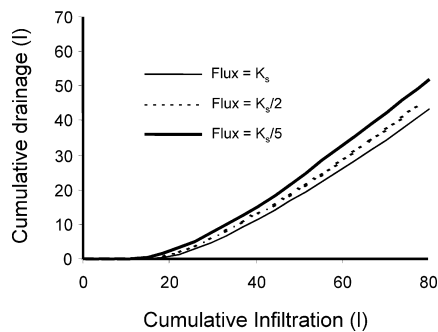
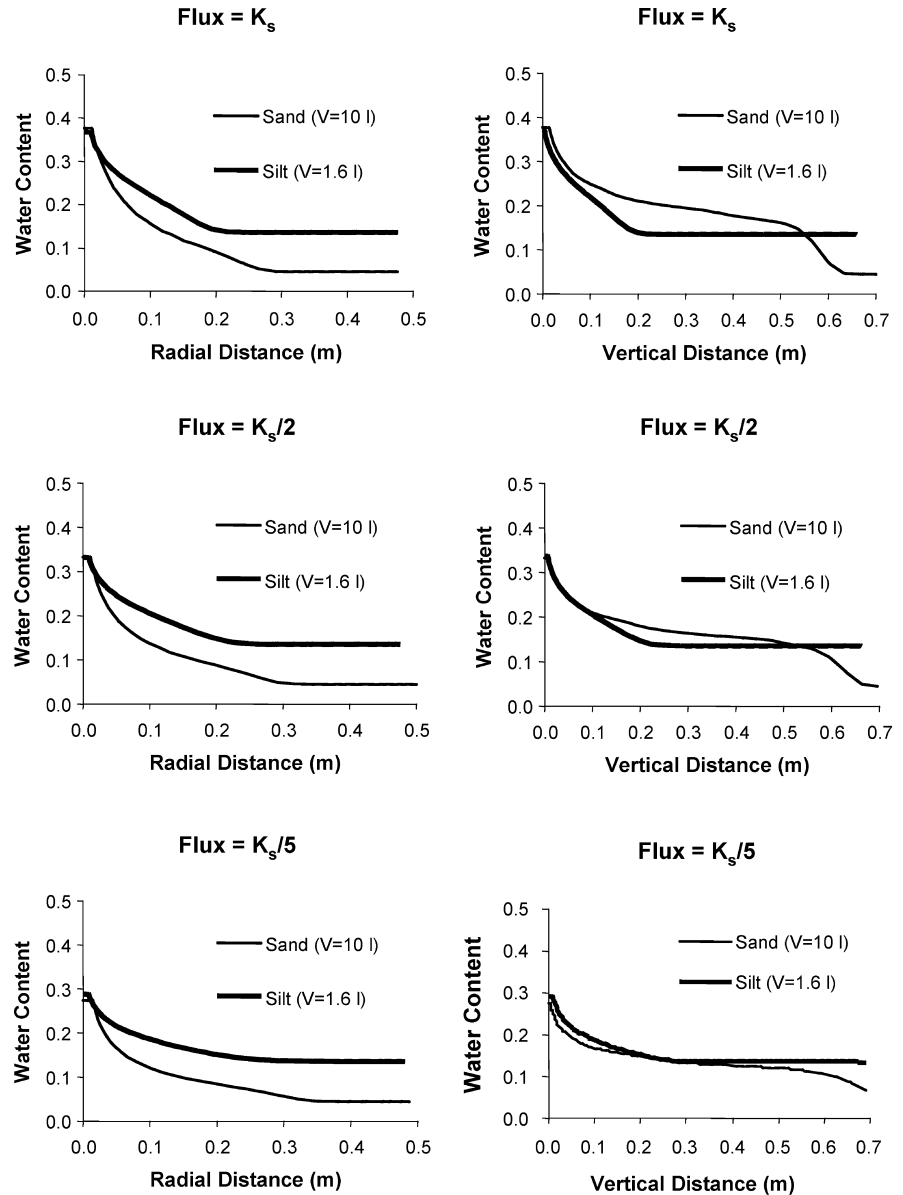


Fig. 10 Cumulative drainage as a function of cumulative infiltration for the highly permeable sand, showing the influence of flow rate on deep drainage

content at the soil surface increases. As water reaches a larger soil surface area, losses by evaporation are likely to increase as well. These results show that off-

site losses, such as evaporation and drainage, can be minimised by choosing appropriate rates of trickle discharge. These simulations suggest that it is possible to control the wetted volume of any particular soil by regulating the trickle discharge according to the hydraulic properties, and that this should be a major goal when designing trickle irrigation systems. Two-dimensional numerical models are a good tool to investigate which combination of hydraulic properties and rate of trickle discharge would yield the best results.

We saw that the risk of deep drainage was greatest in highly permeable coarse-textured soils, and that they were the soils that required most attention in terms of developing appropriate management strategies. In the remainder of the paper, we therefore focus on further analysis of design and management strategies for highly permeable coarse-textured materials.

Influence of irrigation frequency

Figure 11 shows water content distribution at the end of a continuous irrigation event (5 h of continuous water application, see Fig. 3) and at the end of a pulsed irrigation event (water is applied for the first half-hour of each of the ten hours, see Fig. 4). The soil used was the highly permeable sand, and the discharge rate was 1.65 l/h (Flux 1). At the end of both irrigations, the total cumulative infiltration was 8.25 l. Figure 12 shows plots of the water content at $z=30$ cm as a function of the radial distance r , and of the water content at $r=0$ as a function of the vertical distance z at the end of both irrigations. These figures show that pulsed application of water slightly increases the wetted radius of the wetting pattern, contrary to current perceptions. The effect of pulsing was to decrease the average flow rate ($Q=1.65$ l/h applied for 5 h in the case of continuous irrigation, but effectively $Q_p=0.825$ l/h applied for 10 h in the case of pulsed irrigation) and the average water content behind the wetting front $\langle\theta\rangle$, as can be seen in Figs. 11 and 12. The resulting change in the wetted volume depends on both the soil and flow properties. For the wetting fronts

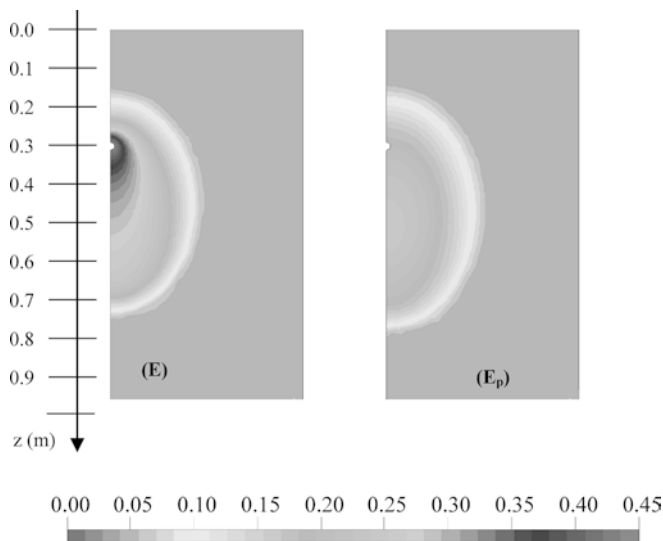
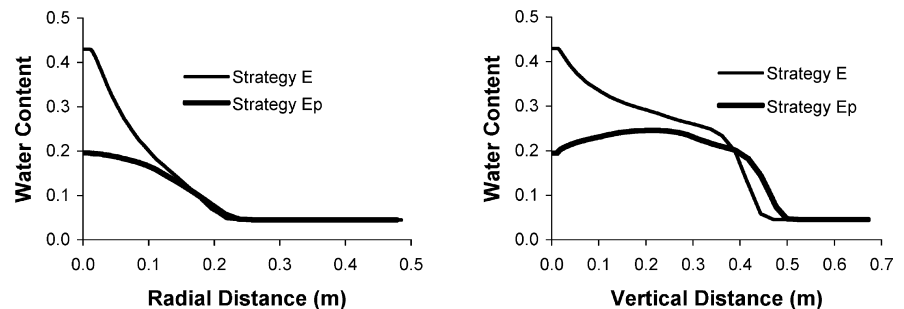


Fig. 11 Simulated water content distribution after 8.25 l of water has been applied either continuously (E) over 5 h, or pulsed over 10 h (E_p)

Fig. 12 Water content at $z=30$ cm as a function of radial distance r , and water content at $r=0$ as a function of vertical distance z at the end of the irrigation event in which 8.25 l of water had been applied



to reach the same distance in the pulsed and continuous irrigations, the dimensionless times need to be the same, so the relationship between the time for the continuous (t) and pulsed irrigations (t_p) needs to be

$$t_p = \frac{Q}{Q_p} \frac{\langle\theta_p\rangle}{\langle\theta\rangle} t = 2 \frac{\langle\theta_p\rangle}{\langle\theta\rangle} t < 2t \quad (22)$$

where $\langle\theta_p\rangle$ is the average water content behind the wetting front for the pulsed irrigation. The same wetted distances for pulsed and continuous irrigation are reached after a cumulative infiltration of $Q_p t_p$, which is less than the cumulative infiltration of $Q t$ at which the water distribution patterns are plotted. With pulsed irrigation, water redistributes between water applications, thereby leading to a slight increase in wetted radius and depth.

Figure 13 shows a plot of cumulative drainage as a function of time for both continuous and pulsed irrigation. At the end of the irrigation cycles, water was left to redistribute for 100 h with HYDRUS2D calculating the drainage during the redistribution period. Results show that after 100 h there is 25% less drainage from the 1 m profile with pulsed irrigation than there is with continuous irrigation.

The wetted distances at $Q t$ in pulsed irrigation are greater than those obtained with continuous irrigation, but $\langle\theta_p\rangle$ is much less than with continuous irrigation. The simulations, however, show that these effects are only marginal and do not seem to warrant application of this pulsed management strategy. However, drainage after 100 h is reduced significantly with pulsed irrigation and this needs to be taken into account when deciding on which irrigation strategy should be used in order to achieve particular goals.

Solute transport under different fertigation strategies

Fertigation strategies E (solute applied at the End of the irrigation cycle) and B (solute applied at the Beginning of irrigation cycle) were simulated for all soils and both continuous and pulsed irrigation (Figs. 3 and 4). Results of these simulations are not shown for the slowly permeable silt and duplex soils, as the timing of solute application had little effect on solute transport. For these soils the water and solutes were held close to the

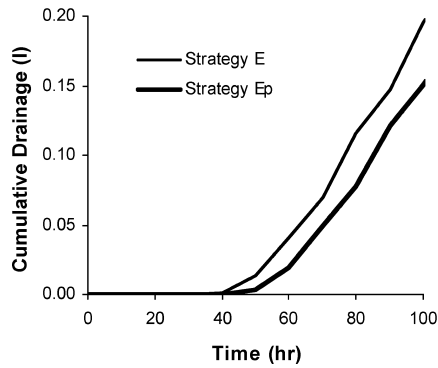


Fig. 13 Cumulative drainage as a function of time for the highly permeable sand

emitter for both fertigation strategies. The maximum depth below the emitter (or height above the emitter in the case of the duplex soil) and width reached by the solute was about 10 cm for both the silt and duplex soil for fertigation strategy E. For fertigation strategy B, these values were slightly less (9 cm). As mentioned earlier, solute leaching is less of an issue in low permeability fine-textured soils than in highly permeable coarse-textured soils.

The fertigation strategy did, however, have a large impact on transport of the mobile non-adsorbed solute (nitrate in this case) in the highly permeable sand. Figure 14 shows the nitrate distribution at $t=10$ h. Note that because nitrate is not applied at the same time for strategy E and B, these patterns show the nitrate distribution 5 h after the end of nitrate application in strategy E, but 9 h after the end of nitrate application in strategy B.

With strategy E, nitrate is applied after the sand has been wetted for 4 h. The concentration patterns are elliptical and nitrate has reached a depth of 90 cm (which is 60 cm below the emitter). In this case 7% of the nitrate is above the emitter plane and 93% below. Further analysis shows that some 22 kg of nitrate per hectare lies at depths between 60 and 90 cm directly below the emitter, as indicated by the zone marked with the dashed line in Fig. 14. This means that for our simulations more than 50% of the applied nitrogen would be at depths greater than 60 cm below the soil surface and could easily be lost to plant uptake.

With strategy B, the concentration patterns show pockets of nitrate forming further away from and above the emitter. In this case 16% of nitrate (more than double the amount for strategy E) is above the emitter. Further analysis shows that for our simulations some 4.4 kg N/ha (11% of the applied solute) is held within the pocket that has formed 10 cm above the emitter. Clearly these nutrients would be more readily available for plant uptake, as they stay in the root zone nearer the soil surface for longer.

The differences in solute (nitrate in our case) concentrations between strategies E and B arise because of the struggle between ‘capillarity’ and ‘gravity’ for control

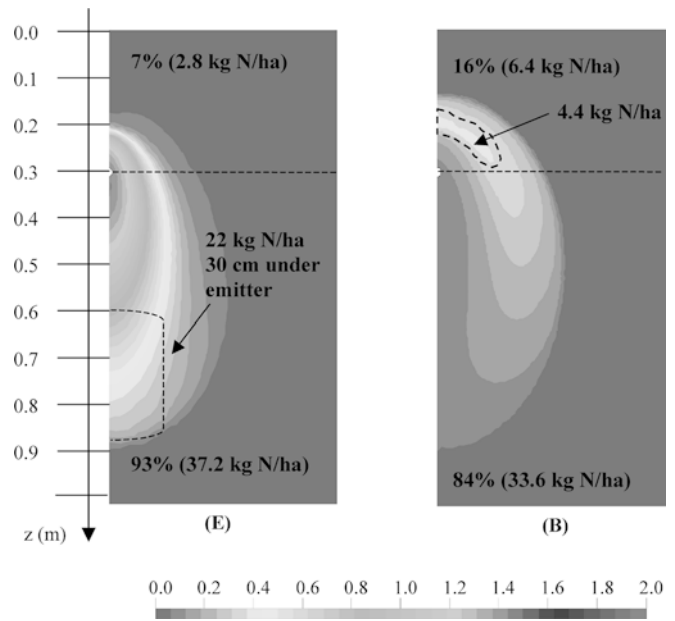


Fig. 14 Simulated nitrate concentration at $t=10$ h in highly permeable sand irrigated using fertigation strategies (E) and (B)

over solute movement. When applying solutes last via strategy E, gravity tends to win out because solutes enter an already wet system and downward flow tends to dominate. When applying solutes first via strategy B, ‘capillarity’ tends to win out, drawing the solutes outwards and upwards from the emitter into the drier soil. As the soil continues to moisten, gravity plays a more important role, exerting a downward pull on the ‘new’ water that is added, but the ‘older’ water with the solutes continues to move outwards and up above the emitter plane in response to capillarity. We can conclude, then, that more solute will be held further from and above the emitter in strategy B than in strategy E, highlighting the lower risk of leaching associated with strategy B, and the potential for greater nutrient use efficiency with this strategy. These results suggest that for the highly permeable sand, strategy B would work better in achieving the goal of increasing nutrient-use efficiency, and reducing the risk of chemical leaching from the root zone.

Conclusions

The results of this study demonstrate that opportunities exist to improve the performance of trickle irrigation systems by adjusting system designs and management strategies to account for differences in soil properties and soil profile features. The simulations showed that hydraulic properties greatly influence the shape and dimensions of the wetting pattern; that decreasing the rate of trickle discharge but keeping the quantity of applied water the same increased the dimensions of the wetting pattern by decreasing the average water content behind the wetting front; that pulsed irrigation resulted in a

slight increase in the dimensions of the wetting pattern but again at lower average water contents; that in highly permeable coarse-textured materials, applying a mobile non-adsorbed solute such as nitrate at the beginning of the irrigation cycle could greatly reduce the risk of solute (e.g. nitrate) leaching; and finally, that a software product providing numerical solutions to the transport equations was a powerful tool for investigating these issues. It should be emphasised that models such as HYDRUS2D capture our current best understanding of how systems work, and that by analysing outputs of these models we can obtain insights into how design and management strategies could be improved. Having said this, though, we still need to continually question the validity of our current understanding and seek ways to improve it.

We believe that further improvements to this work will require more targeted fieldwork to complement progress with the modelling and scenario analyses. This fieldwork should aim to provide improved measurements of soil hydraulic and solute transport properties, and improved measurements of the movement and fate of nutrients and agrochemicals applied via fertigation. Areas that require particular attention include:

- Integration of chemical interactions and reactions and biological processes within the overall irrigation system. This will require appropriate field and laboratory data to facilitate this work.
- Analysis of the influence of soil structure on solute transport, and design of fertigation strategies that enable solutes to be held by the soil structure rather than flushed down preferential flow pathways.
- Analysis of interactions between trickle irrigation and rainfall. This could involve probabilistic studies to determine the likely impacts of various management strategies within particular climatic zones.
- Analysis of the interactions between trickle irrigation/fertigation and plant water uptake. The rates of uptake and downward movement of nutrients need to be studied to ensure that supply is matched to demand and that there is little or no excess of nutrients within the root zone that can be leached.
- Analysis of the impact of different emitter designs and geometries. Our simulation results showed water and solute movement for the specific case of a 1 cm diameter circular emitter applying a uniform flow rate in all directions. Results obtained will differ somewhat with different designs, and emitters with an impervious 'base' which only supply water and solute towards the top of the profile would probably achieve better results than those that only supply water downwards

If trickle irrigation is to provide the benefits expected of it, there is a clear need to make better use of soil properties and soil profile information to provide more efficient and robust irrigation and fertigation guidelines. The aim must be to ensure that solutes (nutrients and agrochemicals) are held within the soil structure within

the root zone to maximise plant uptake opportunities and minimise drainage and leaching.

Acknowledgements This work was supported in part by CSIRO, Land and Water Australia through its National Program on Irrigation Research and Development (NPIRD), and the CRC for Sustainable Sugar Production.

References

- Bear J (1972) Dynamics of fluids in porous media. Elsevier, New York
- Beven KJ, Henderson DE, Reeves AD (1993) Dispersion parameters for undisturbed partially saturated soil. *J Hydrol* 143: 19–43
- Brandt A, Bresler E, Diner N, Ben-Asher I, Heller J, Goldberg D (1971) Infiltration from a trickle source. I. Mathematical models. *Soil Sci Soc Am Proc* 35:675–682
- Bresler E (1975) Two-dimensional transport of solutes during nonsteady infiltration from a trickle source. *Soil Sci Soc Am Proc* 39:604–613
- Bresler E (1977) Trickle-drip irrigation: principles and application to soil-water management. *Adv Agron* 29:343–393
- Bresler E (1978) Analysis of trickle irrigation with application to design problems. *Irrig Sci* 1:3–17
- Bresler E, Heller J, Diner N, Ben-Asher I, Brandt A, Goldberg D (1971) Infiltration from a trickle source. II. Experimental data and theoretical predictions. *Soil Sci Soc Am Proc* 35:683–689
- Bristow KL, Cote CM, Thorburn PJ, Cook FJ (2000) Soil wetting and solute transport in trickle irrigation systems. In: 6th international micro-irrigation conference (Micro2000), 22–27 October 2000, Cape Town, South Africa
- Clothier BE, Scotter DR (1982) Constant-flux infiltration from a hemispherical cavity. *Soil Sci Soc Am J* 46:696–700
- Coelho FE, Or D (1997) Applicability of analytical solutions for flow from point sources to drip irrigation management. *Soil Sci Soc Am J* 61:1331–1341
- Cote CM, Bristow KL, Ford E-J, Verburg K, Keating B (2001) Measurement of water and solute movement in large undisturbed soil cores: analysis of Macknade and Bundaberg data. CSIRO Land and Water, Technical Report 07/2001
- Genuchten MTh van (1980) A closed form equation for predicting the hydraulic conductivity of unsaturated soils. *Soil Sci Soc Am J* 44:892–898
- Hanson B, Schwankl L, Grattan S, Prichard T (1996) Drip irrigation for row crops: water management handbook series. (Publication 93–05) University of California-Davis, Calif.
- Lafolie F, Guennelon R, Genuchten MTh van (1989a) Analysis of water and flow under trickle irrigation. I. Theory and numerical solution. *Soil Sci Soc Am J* 53:1310–1318
- Lafolie F, Guennelon R, Genuchten MTh van (1989b) Analysis of water and flow under trickle irrigation. II. Experimental evaluation. *Soil Sci Soc Am J* 53:1318–1323
- Philip JR (1968) Steady infiltration from buried point sources and spherical cavities. *Water Resour Res* 4:1039–1047
- Philip JR (1984) Travel times from buried and surface infiltration point sources. *Water Resour Res* 20:990–994
- Raats PAC (1971) Steady infiltration from point sources, cavities, and basins. *Soil Sci Soc Am Proc* 35:689–694
- Rawlins SL (1973) Principles of managing high frequency irrigation. *Soil Sci Soc Am Proc* 37:626–629
- Revol P, Clothier BE, Mailhol J-C, Vachaud G, Vauclin M (1997) Infiltration from a surface point source and drip irrigation. 2. An approximate time-dependent solution for wet-front position. *Water Resour Res* 33:1869–1874
- Simunek J, Sejna M, Genuchten MTh van (1999) HYDRUS-2D/MESHGEN-2D: simulating water flow and solute transport in two-dimensional variably saturated media. International Groundwater Modeling Centre, Colorado School of Mines, Golden, Colo.

- Thorburn PJ, Cook FJ, Bristow KL (2000) Variations in wetting patterns from trickle emitters in soils of different texture. In: 6th international micro-irrigation conference (Micro2000), 22–27 October 2000, Cape Town, South Africa
- Warrick AW (1974) Time-dependent linearized infiltration. I. Point sources. *Soil Sci Soc Am Proc* 38:383–386
- Warrick AW, Lomen DO (1976) Time-dependent linearized infiltration. III. Strip and disc sources. *Soil Sci Soc Am J* 40:639–643
- Weast RC (ed) (1978) *Handbook of chemistry and physics*, 58th edn. CRC, Boca Raton, Fla.
- White I, Sully MJ (1987) Macroscopic and microscopic capillarity length and time scales from field infiltration. *Water Resour Res* 23:1514–1522
- Wooding RA (1968) Steady infiltration from a shallow circular pond. *Water Resour Res* 4:1259–1273